

## Intra-day variability of BL Lacertae from 2016 to 2018

Tian Li, Jiang-Hua Wu, Nan-Kun Meng, Yan Dai and Xiao-Yuan Zhang

Department of Astronomy, Beijing Normal University, Beijing 100875, China; [jhwu@bnu.edu.cn](mailto:jhwu@bnu.edu.cn)

Received 2021 June 10; accepted 2021 July 9

**Abstract** We monitored BL Lacertae in the  $B$ ,  $V$ ,  $R$  and  $I$  bands for 14 nights during the period of 2016–2018. The source showed significant intra-day variability on 12 nights. We performed color-magnitude analysis and found that the source exhibited bluer-when-brighter chromatism. This bluer-when-brighter behavior is at least partly caused by the larger variation amplitude at shorter wavelengths. The variations at different wavelengths are correlated well and show no inter-band time lag.

**Key words:** galaxies: active — BL Lacertae objects: individual: BL Lacertae — galaxies: photometry

### 1 INTRODUCTION

A blazar is the most violently variable object among all kinds of active galactic nuclei (AGNs). The relativistic jets of blazars are believed to be oriented close to the line of our sight and be powered by the central accretion disk of supermassive black hole systems. BL Lacertae objects (BL Lacs) and flat-spectrum radio quasars (FSRQs) are subsets of blazars. BL Lacs are named after the well-known blazar called BL Lacertae, which is characterized by its high and variable polarization, absence of strong emission lines in the optical spectrum, synchrotron emission from relativistic jets, and intense flux and spectral variability from radio to  $\gamma$ -ray on a wide variety of timescales (Wagner & Witzel 1995; Böttcher et al. 2003). For intra-day variability (IDV), the flux can change over hundredths or even tenths of a magnitude within several hours (Agarwal & Gupta 2015). A blazar’s spectral energy distribution (SED) displays two peaks (Fossati et al. 1998). We can divide BL Lacs into three classes based on the locations of these peaks. For the high-energy-peaked BL Lacs (HBLs), their first peaks are located in ultraviolet/X-rays while the second peaks are located at TeV energies. The synchrotron emission peaks of an intermediate-frequency-peaked BL Lac (IBL) lie in the optical region. BL Lacertae is a low-frequency-peaked BL Lac (LBL) (Ciprini et al. 2004; Abdo et al. 2010) as its first component peaks at infrared while its second component peaks around MeV-GeV (Padovani & Giommi 1995; Abdo et al. 2010).

BL Lacertae, hosted in a giant elliptical galaxy with  $R = 15.5$  mag (Scarpa et al. 2000), has a redshift of  $z = 0.0668 \pm 0.0002$  (Miller & Hawley 1977). It

was once observed in several multiwavelength campaigns carried out by the Whole Earth Blazar Telescope/GLAST-AGILE Support Program (WEBT/GASP) (Villata et al. 2004b; Bach et al. 2006; Raiteri et al. 2009). Some other investigations have been conducted to study its flux variations, spectral changes and inter-band cross-correlations (Epstein et al. 1972; Carini et al. 1992; Villata et al. 2002; Papadakis et al. 2003; Zhai & Wei 2012; Agarwal & Gupta 2015; Gaur et al. 2015; Meng et al. 2017; Bhatta & Webb 2018; Sadun et al. 2020). Most of the observations found its amplitude of IDV is larger at a shorter wavelength. The IDV amplitude is usually larger when the duration of the observation is longer (Gupta & Joshi 2005; Gaur et al. 2015, 2017). The IDV amplitude also decreases as the source flux increases (Gaur et al. 2015, 2017). The reason might be that the irregularities in the turbulent jet will decrease when the source is at a bright state and fewer non-axisymmetric bubbles were carried downward in the relativistic jets (Marscher 2014; Gaur et al. 2015). Sandrinelli et al. (2018) identified possible  $\gamma$ -ray and optical correlated quasi-periodicities of 1.86 yr. The bluer-when-brighter (BWB) trend was found in previous observations. The BWB trend tends to appear on short timescales rather than on long timescales, indicating that there are probably two different components in the variability of BL Lacertae (Villata et al. 2002, 2004a). Although BL Lacs usually exhibit BWB trends, redder-when-brighter (RWB) trends are frequently seen in FSRQs (Li et al. 2018; Gupta et al. 2019). The variations in different bands are highly correlated. Several authors found time lag between variations in different bands of BL Lacertae. For example, Papadakis et al. (2003)

ascertained a delay of 0.4 h between the *B* and *I* bands. Hu et al. (2006) reported a delay of 11.6 min between the *e* and *m* bands. A possible time lag of 11.8 min between the *R* and *V* bands was reported by Meng et al. (2017).

In this paper, we aim to study the optical IDV and spectral variations of BL Lacertae. We carried out photometric measurement of this object on 14 nights in 2016–2018. We also tried to find any possible inter-band time lags in order to study the physical nature of the acceleration and cooling mechanisms in the relativistic jet and the origin of IDV. The paper is organized as follows. In Section 2, we describe our observations and data reductions. Section 3 explains the analysis techniques followed by results. Section 4 gives the conclusions.

## 2 OBSERVATIONS AND DATA REDUCTIONS

The observations were carried out on 14 nights in the period from 2016 November 3 to 2018 December 3. We used an 85 cm reflector to do the observations. It is at Xinglong Station, National Astronomical Observatories, Chinese Academy of Science (NAOC). The telescope incorporates a primary focus system (F/3.27) with an Andor CCD and Johnson and Cousins filters *UBVRI*. The CCD has 2048×2048 pixels and the pixel size is 12 μm.

The photometric observations were performed in the *B*, *V*, *R* and *I* bands, and we chose different combinations of filters on different observations (see Table 1). The camera was switched to a cyclical mode for the exposures. In order to get enough signal to noise ratio (SNR), the exposure times were set according to the filter, weather condition, seeing, moon phase and atmospheric transparency. They ranged from 8 to 120 s. The observation log is displayed in Table 1. Figure 1 shows the finding chart.

We utilized IRAF to reduce the data. The procedures included bias subtraction, flat fielding, extraction of instrumental aperture magnitude and flux calibration. The average full width at half maximum (FWHM) of the stellar images varied between 2 and 4 arcsec from night to night. After a few trials with different aperture sizes, we adopted an aperture size of 1.5 times the average FWHM of the stellar images. The inner and outer radii of the sky annuli were adopted as 5 and 7 times the stellar FWHM, respectively. The magnitudes of BL Lacertae were calibrated with respect to the magnitude of star 3 in Figure 1. Star 6 is selected as the check star. Its magnitudes were also calibrated and were used to check the accuracy of our observations. Star 2 and stars 4–8 were selected and used in the quantitative assessment of the IDV, as will be described in the next section. Their magnitudes were calibrated relative to the brightness of star 3. The standard

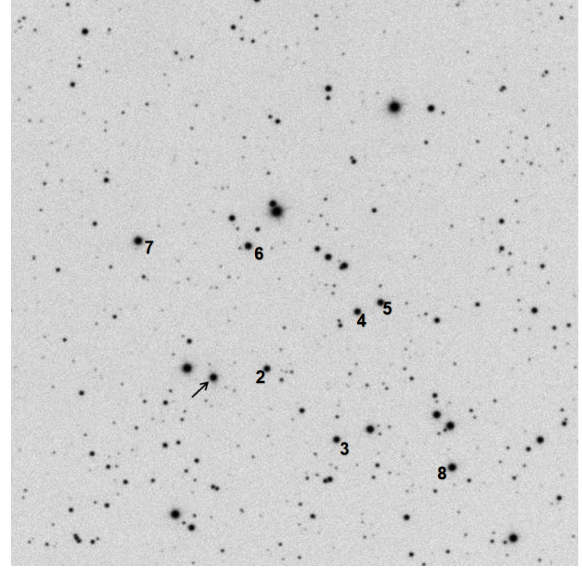


**Fig. 1** Finding chart of BL Lacertae in *R* band. The images were taken on 2016 November 3. BL Lacertae is marked by an *arrow*. Star 6 is the check star, star 2 and stars 4–8 were selected and used in the quantitative assessment of the IDV. Their magnitudes were all calibrated relative to the brightness of star 3.

magnitudes of stars 3, 4 and 6 in the *B*, *V*, *R* and *I* bands are reported by Smith et al. (1985).

The photometric errors from IRAF are significantly underestimated according to Goyal et al. (2013). Their method is to determine a coefficient  $\eta$  which is the ratio between the real photometric error and that given by IRAF. Here we selected the check star (star 6) due to its lowest fluctuations and calculate  $\chi^2$  by relying on the equation

$$\chi^2 = \sum_{i=1}^N \frac{(V_i - \bar{V})^2}{\sigma_i^2}. \quad (1)$$

In this equation,  $V_i$  is the  $i$ th differential magnitude,  $\bar{V}$  is the mean of all differential magnitudes and  $\sigma_i$  is the original error given by IRAF. The degree of freedom  $\nu$  can be calculated from

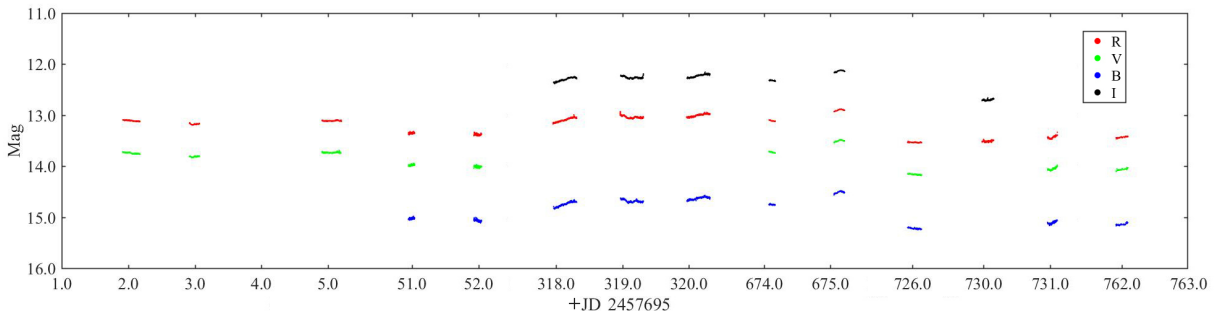
$$\nu = N - 1 = \chi^2 / \eta^2. \quad (2)$$

Then we obtained the regression analysis with fixed slope to calculate the coefficient  $\eta$ . See Goyal et al. (2013) for more details.

We calculated  $\eta$  for each band in each day and found that  $\eta$  ranges from 1.0764 to 1.7367, which is used to modify the original errors obtained by IRAF.

**Table 1** Observation Log

Julian Date (JD)	Date (yyyy mm dd)	Passband	Data points	Exposure time (s)	Duration (h)
2457696	2016 11 03	V	160	60	6.2
		R	160	60	6.2
2457697	2016 11 04	V	94	60	3.6
		R	93	60	3.6
2457699	2016 11 06	V	178	60	7.0
		R	181	60	7.0
2457745	2016 12 22	B	97	30	2.3
		V	97	20	2.3
		R	95	8	2.2
2457746	2016 12 23	B	103	40	2.8
		V	101	18	2.8
		R	101	10	2.8
2458012	2017 09 15	B	232	60	8.3
		R	250	20	8.5
		I	233	20	8.3
2458013	2017 09 16	B	235	60	8.2
		R	235	20	8.4
		I	232	20	8.1
2458014	2017 09 17	B	230	60	8.3
		R	236	20	8.5
		I	228	20	8.3
2458369	2018 09 07	B	31	60	2.3
		V	31	60	2.3
		R	31	60	2.3
		I	31	60	2.3
2458370	2018 09 08	B	52	60	3.8
		V	52	60	3.8
		R	52	60	3.8
		I	52	60	3.8
2458420	2018 10 28	B	67	60	5.1
		V	68	60	5.1
		R	68	60	5.0
2458424	2018 11 01	R	132	50	4.2
		I	132	40	4.2
2458425	2018 11 02	B	84	20	3.5
		V	84	40	3.5
		R	84	60	3.5
2458456	2018 12 03	B	51	120	4.3
		V	51	60	4.3
		R	51	60	4.2

**Fig. 2** Light curves of BL Lacertae in the *B*, *V*, *R* and *I* bands in 3 yr. Different colored dots represent data in different bands.

### 3 RESULTS

#### 3.1 Light Curves

The overall light curves are displayed in Figure 2. The light curves exhibit obvious long term fluctuations. The largest amplitude of *R* band is about 0.6 mag.

The intra-night light curves of the object are plotted in Figure 3. Heidt & Wagner (1996) developed a method to quantify the IDV amplitude

$$A = \sqrt{(m_{\max} - m_{\min})^2 - 2\sigma^2}, \quad (3)$$

where  $\sigma$  is the measurement error. According to Equation (3), the value  $A$  will always be larger than 0,

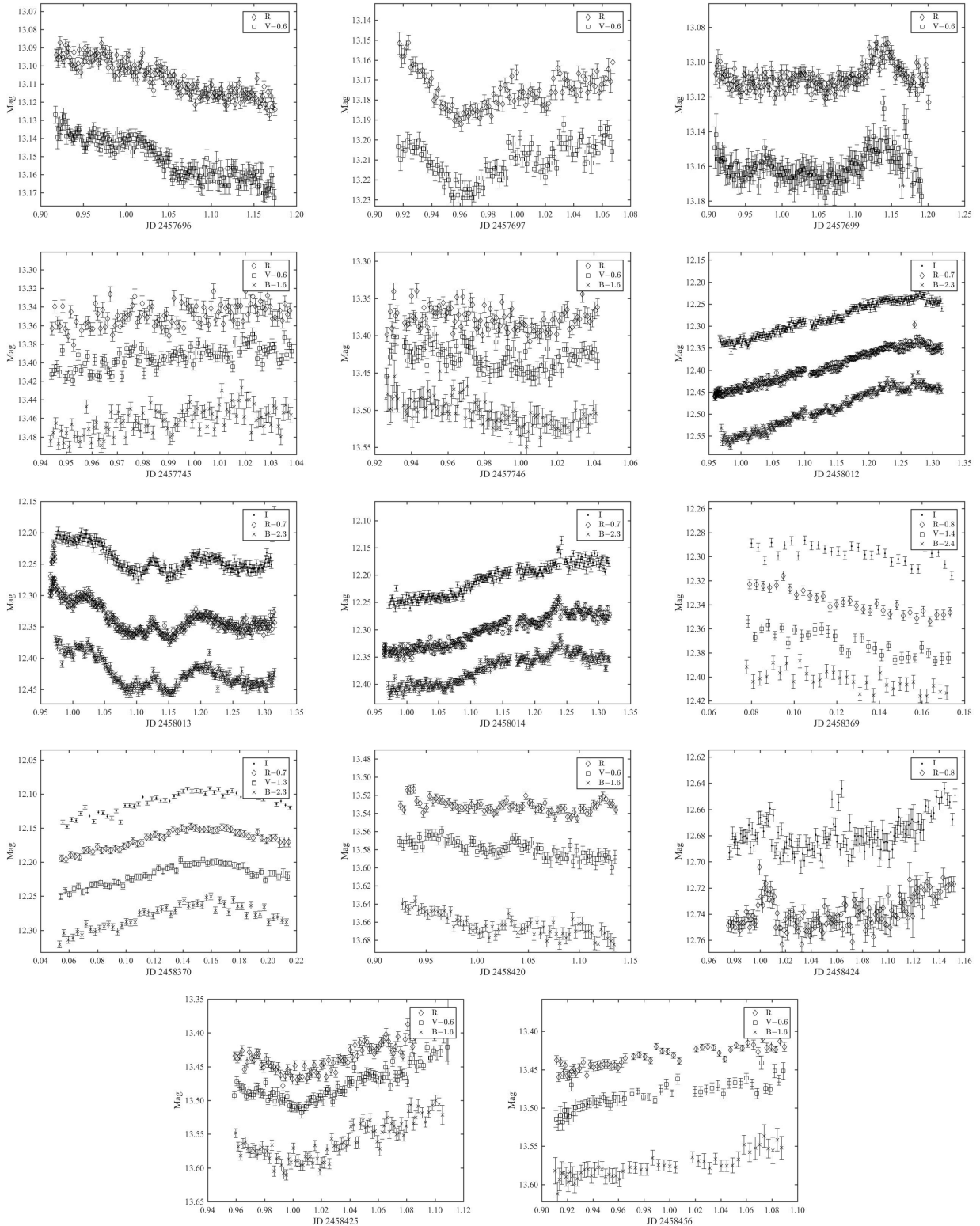


**Fig. 3** Intra-day light curves. For clarity, the  $B$ ,  $V$ ,  $R$  and  $I$  light curves are shifted. The shifted magnitudes are given in the plots.

however it does not mean that the corresponding light curve is variable. The most violent variation happened on JD 2458012 (2017 September 15) when the IDV amplitude

reached 16.5% (0.17 mag) in the  $B$  band and the variation rate was  $0.3 \text{ mag hr}^{-1}$ . On JD 2458014 (2017 September 17) the object reached its brightest state of  $R = 12.95 \text{ mag}$ ,

while on JD 2458420 (2018 October 28) the object was at its faintest state with  $R = 13.55$  mag. The IDV amplitude for each band in each night is included in Table 2. Figure 4 plots the IDV amplitudes of the variable light curves. According to Figure 4 and Table 2, the IDV amplitude is greater in higher energy bands. The IDV amplitude is comparable in a few cases where the differences between IDV amplitude are smaller than 0.5%. This trend has also been observed by others (e.g., Nesci et al. 1998; Webb et al. 1998; Fan & Lin 1999; Nikolashvili & Kurtanidze 2004; Meng et al. 2017).

### 3.2 Variability Detection

We performed the nested analysis of variance (ANOVA) and enhanced  $F$ -test to examine and quantify the IDV (de Diego et al. 2015).

In the nested ANOVA analysis, we separated the data points of a certain band on a certain day into groups, with five data points in each group. The null hypothesis is that the deviation of the mean values of differential light curves in each group is zero. The expressions for the degrees of freedom and  $F$ -value are shown in equation (4) in de Diego et al. (2015).

The enhanced  $F$ -test uses several comparison field stars. First, the errors of the field stars are scaled into our target’s level. By fitting an exponential curve to our comparison stars, we can obtain the relationship between the standard deviation and the mean magnitude of the light curve. This relationship can be utilized to transfer the error of field stars into the level of BL Lacertae. At last, we subtract the mean magnitude from each field star’s light curve and stack them together. The  $F$ -value is the variance of BL Lacertae’s curve divided by the variance of the stacked light curve.

### 3.3 Variation Result

The results of the two tests are listed in Table 2.  $\nu_1$  and  $\nu_2$  are degrees of freedom in each test. Column (15) is the IDV amplitude. Column (14) is the variability.  $F_{\text{crit}}$  is the critical value of the  $F$ -test at  $\alpha = 0.05$  ( $\alpha$  is significance level). When the light curve’s  $F$ -value is larger than  $F_{\text{crit}}$  and its  $p$ -value is smaller than 0.05, the light curve passes the test. If the light curve passes both tests, BL Lacertae will be marked as ‘Y’ (Yes). ‘N’ (No) means the light curve did not pass at least one of the tests. Twenty-three light curves on twelve nights are variable according to both tests, but three did not pass both tests. Fourteen light curves passed one of the tests but as their  $p$ -value of the other test is larger than 0.05, we cannot determine their variability, so we marked them as ‘P’ (Possible). Small flares can be seen in the  $V$  band on 2016 November 4 (JD 2457697) and

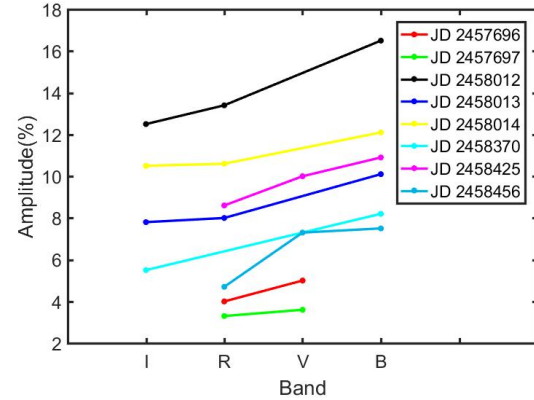


Fig. 4 The IDV amplitudes of the variable light curves.

2016 November 6 (JD 2457699), and all bands on 2018 October 28 (JD 2458420). Due to the measurement error, these light curves only passed one of the tests but are still very likely variable.

### 3.4 Inter-band Correlation Analysis and Time Lags

To search for the possible time lags between variations in different bands, we performed cross-correlation analyses. Two cross-correlation methods are considered. One is the z-transformed discrete correlation functions (ZDCFs) (Alexander 1997, 2013), in which equal population binning and Fisher’s z-transform are used to correct several biases of the discrete correlation function of Edelson & Krolik (1988). A Gaussian fitting (GF) of the ZDCF points greater than 75% of the peak value can give an estimate of the time lag and the associated errors. However, GF may underestimate the error (e.g., Wu et al. 2012). So we only take the results of the ZDCF+GF method as a reference. For a more reliable estimate of the time lags and errors, we relied on the interpolated cross-correlation function (ICCF) (Gaskell & Peterson 1987). Peterson et al. (1998, 2004) employed a Monte Carlo (MC) method to calculate the centroid position of the ICCF and its error. Flux randomization (FR) and random-subset selection (RSS) are applied in each MC realization. Here we performed 5000 MC realizations. The results are listed in Table 3. On 2018 December 3 (JD 2458456), the GF failed to fit the ZDCF, so the results are not listed in the table.

According to our results, no time lag has significance greater than  $3\sigma$ , thus we failed to detect any time lags at high significance in our observations.

### 3.5 Color Variations

By calculating the color indices of  $B - R$ ,  $V - R$ ,  $V - I$  and  $B - I$ , we investigated the color variation with respect to the magnitude of BL Lacertae for each night.

**Table 2** IDV Test Results

Julian Date (JD)	Date	Filter	Enhanced $F$ -test					Nested ANOVA					Variability	Amplitude
			$F$	$\nu_1$	$\nu_2$	$F_{\text{crit}}$	$P$	$F$	$\nu_1$	$\nu_2$	$F_{\text{crit}}$	$P$		
(1)	(2)	(3)	(4)	(5)	(6)	(7)	(8)	(9)	(10)	(11)	(12)	(13)	(14)	(15)
2457696	2016 11 03	V	3.67	160	800	1.21	< 0.0001	5.10	31	159	1.83	< 0.0001	Y	5.0
		R	5.89	160	800	1.21	< 0.0001	2.46	31	159	1.83	< 0.0001	Y	4.0
2457697	2016 11 04	V	3.02	94	470	1.28	< 0.0001	1.92	17	89	2.21	< 0.0001	Y	3.6
		R	6.52	93	465	1.29	< 0.0001	3.79	17	89	2.21	< 0.0001	Y	3.3
2457699	2016 11 06	V	1.08	178	890	1.21	< 0.0001	2.28	18	94	1.79	0.0082	N	
		R	0.11	181	905	1.25	0.9999	1.51	19	99	1.77	0.1044	N	
2457745	2016 12 22	B	1.89	97	485	1.28	< 0.0001	1.14	18	94	2.21	0.3297	P	5.4
		V	2.80	97	485	1.28	< 0.0001	0.48	18	94	2.21	0.9584	P	4.1
		R	2.06	95	475	1.28	< 0.0001	1.06	18	94	2.21	0.4118	P	7.5
2457746	2016 12 23	B	1.36	103	515	1.27	0.0165	3.08	19	99	2.12	< 0.0001	Y	10.6
		V	2.10	101	505	1.27	< 0.0001	1.29	19	99	2.12	0.0686	P	7.5
		R	2.28	101	505	1.27	< 0.0001	1.41	19	99	2.12	0.5124	P	7.4
2458012	2017 09 15	B	20.15	232	1160	1.18	< 0.0001	8.46	45	229	1.66	< 0.0001	Y	16.5
		R	28.59	250	1250	1.17	< 0.0001	8.07	49	249	1.63	< 0.0001	Y	13.4
		I	28.69	233	1165	1.18	< 0.0001	7.43	45	229	1.66	< 0.0001	Y	12.5
2458013	2017 09 16	B	7.99	235	1175	1.17	< 0.0001	3.33	46	234	1.66	< 0.0001	Y	10.1
		R	13.87	255	1275	1.17	< 0.0001	3.61	50	254	1.63	< 0.0001	Y	8.0
		I	6.14	232	1160	1.18	< 0.0001	3.62	45	229	1.66	< 0.0001	Y	7.8
2458014	2017 09 17	B	6.46	230	1150	1.18	< 0.0001	2.45	45	229	1.66	< 0.0001	Y	12.1
		R	12.56	236	1180	1.17	< 0.0001	2.74	46	234	1.66	< 0.0001	Y	10.6
		I	16.54	228	1140	1.18	< 0.0001	4.89	44	224	1.68	< 0.0001	Y	10.5
2458369	2018 09 07	B	1.02	31	155	1.53	0.4436	1.56	5	29	2.62	0.2106	N	
		V	4.44	31	155	1.53	< 0.0001	2.02	5	29	2.62	0.1123	P	3.3
		R	4.76	31	155	1.53	< 0.0001	6.94	5	29	2.62	0.0003	Y	3.2
		I	4.88	31	155	1.53	< 0.0001	1.25	5	29	2.62	0.3176	P	3.3
2458370	2018 09 08	B	8.00	52	260	1.40	< 0.0001	4.29	9	49	2.12	0.0006	Y	8.2
		V	8.66	52	260	1.40	< 0.0001	1.96	9	49	2.12	0.0706	P	5.6
		R	14.22	52	260	1.40	< 0.0001	1.59	9	49	2.12	0.1523	P	4.9
		I	27.30	52	260	1.40	< 0.0001	3.50	9	49	2.12	0.0028	Y	5.5
2458420	2018 10 28	B	2.37	67	335	1.34	< 0.0001	1.66	12	64	1.94	0.1040	P	5.6
		V	3.01	68	340	1.34	< 0.0001	1.49	12	64	1.94	0.1597	P	4.4
		R	3.81	68	340	1.34	< 0.0001	0.99	12	64	1.94	0.4700	P	3.3
2458424	2018 11 01	R	2.64	132	660	1.24	< 0.0001	1.09	25	129	1.94	0.3716	P	6.3
		I	3.87	132	660	1.24	< 0.0001	3.93	25	129	1.94	0.0008	Y	6.4
2458425	2018 11 02	B	4.31	84	420	1.30	< 0.0001	2.82	15	79	2.31	0.0020	Y	10.9
		V	7.12	84	420	1.30	< 0.0001	4.28	15	79	2.31	< 0.0001	Y	10.0
		R	7.28	84	420	1.30	< 0.0001	2.50	15	79	2.31	0.0046	Y	8.6
2458456	2018 12 03	B	1.52	51	255	1.40	0.0195	6.27	9	49	2.12	< 0.0001	Y	7.5
		V	7.32	51	255	1.40	< 0.0001	4.99	9	49	2.12	0.002	Y	7.3
		R	7.73	51	255	1.40	< 0.0001	2.25	9	49	2.12	0.0382	Y	4.7

A linear fit was made to the data points. The examples of color-magnitude diagrams are displayed in Figure 5. The scales of the horizontal axis and vertical axis are fixed as 0.2 and 0.1 mag, respectively in order to make comparison convenient between panels.

We calculated the Spearman correlation coefficient ( $Sc$ ) and the corresponding  $p$ -value. The results are displayed in Table 4. The first and second columns are

the date of observation, the third and fourth columns are the passbands of color index, and the fifth column is the number of datapoints followed by  $Sc$  value and corresponding  $p$ -value. The last column is the strength of correlation. The bands without variation are not shown in this table because it is pointless to discuss their trend. The numbers of data points of our color-magnitude diagrams are all above 31. The critical value of the correlation

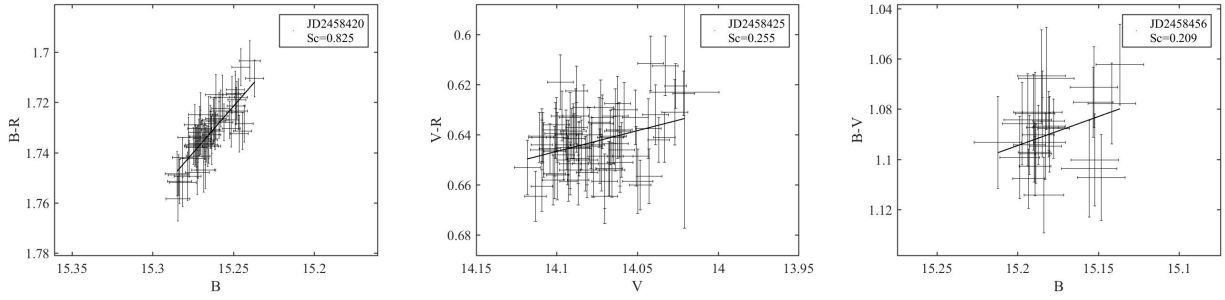


**Fig. 5** Examples of intranight color-magnitude diagrams, which illustrate strong, mild and weak correlations from the left panel to the right panel respectively.

**Table 3** Time Lags from Correlation Analyses

Julian Date (JD)	Date (yyyy mm dd)	Passbands	ZDCF–GF (min)	ICCF–FR/RSS (min)
2457696	2016 11 03	$R - V$	$-28.86 \pm 9.13$	$-22.62 \pm 29.01$
2457697	2016 11 03	$R - V$	$-7.07 \pm 5.29$	$-5.73 \pm 6.18$
2457699	2016 11 06	$R - V$	$-15.59 \pm 4.49$	$-5.69 \pm 5.05$
2457745	2016 12 22	$R - V$	$-8.02 \pm 10.63$	$-6.03 \pm 38.42$
		$R - B$	$-11.68 \pm 7.67$	$-18.56 \pm 36.13$
		$V - B$	$-3.90 \pm 1.94$	$-4.08 \pm 25.57$
2457746	2016 12 23	$R - V$	$-2.77 \pm 4.78$	$-2.14 \pm 9.12$
		$R - B$	$+7.49 \pm 4.34$	$+10.67 \pm 13.58$
		$V - B$	$+10.40 \pm 6.24$	$+12.45 \pm 12.76$
2458012	2017 09 15	$R - I$	$-7.63 \pm 3.35$	$-3.34 \pm 4.54$
		$R - B$	$-23.87 \pm 5.24$	$-2.61 \pm 6.18$
		$I - B$	$-0.38 \pm 3.16$	$+2.22 \pm 3.51$
2458013	2017 09 16	$R - I$	$+4.05 \pm 1.29$	$-1.63 \pm 4.45$
		$R - B$	$+2.54 \pm 1.05$	$+0.13 \pm 3.93$
		$I - B$	$+2.00 \pm 0.74$	$+2.85 \pm 2.63$
2458014	2017 09 17	$R - I$	$-2.25 \pm 2.92$	$+5.59 \pm 6.88$
		$R - B$	$-9.74 \pm 2.63$	$-3.86 \pm 8.64$
		$I - B$	$-0.44 \pm 8.97$	$-7.13 \pm 5.92$
2458369	2018 09 07	$B - R$	$-15.37 \pm 7.08$	$-15.11 \pm 29.98$
		$B - V$	$-4.68 \pm 10.73$	$-3.62 \pm 32.65$
		$B - I$	$+11.53 \pm 5.33$	$+7.02 \pm 36.80$
2458370	2018 09 08	$B - R$	$+2.20 \pm 4.78$	$+1.30 \pm 7.27$
		$B - V$	$+1.56 \pm 4.36$	$+0.41 \pm 7.47$
		$B - I$	$+6.15 \pm 5.5$	$+3.04 \pm 6.52$
2458420	2018 10 28	$R - V$	$+33.49 \pm 9.74$	$+20.02 \pm 91.25$
		$R - B$	$+19.22 \pm 6.94$	$+16.63 \pm 92.97$
		$V - B$	$-16.86 \pm 11.63$	$-57.09 \pm 66.31$
2458424	2018 11 01	$R - I$	$-5.4 \pm 4.05$	$-0.58 \pm 3.21$
2458425	2018 11 02	$R - V$	$-2.39 \pm 1.07$	$-1.70 \pm 6.34$
		$R - B$	$-4.47 \pm 1.16$	$+1.69 \pm 6.36$
		$V - B$	$-2.87 \pm 1.41$	$-1.20 \pm 6.56$
2458456	2018 12 03	$R - V$		$+28.94 \pm 53.46$
		$R - B$		$-10.22 \pm 33.68$
		$V - B$		$+19.81 \pm 46.77$

coefficient is 0.442 at the significance level of 0.01 and degree of freedom of 31. Most of our Sc values of color-magnitude diagrams are above 0.344 with  $p$ -value lower than 0.0001, indicating strong correlations. On 2017 September 17 (JD 2458014), the Sc values of all the color-magnitude diagrams are lower than the critical values with  $p$ -values larger than 0.01, and we regard them as having no correlations. On 2018 October 28 (JD 2458420) the Sc value of the  $B$ - $R$  diagram is 0.820 with a  $p$ -value significantly smaller than 0.01, indicating a strong BWB color behavior. For the rest, the Sc value ranges from 0.4

to 0.6 with  $p$ -value smaller than 0.001. In the  $B$  and  $R$  bands of 2018 December 3 (JD 2458456), and  $R$  and  $V$  bands of 2018 December 3 (JD 2458456), the light curves are not correlated.

According to Ikejiri et al. (2011), we do not know if the BWB trend is universal in blazars. There are two types of blazars, BL Lacs and FSRQs. The BWB trend is often observed in BL Lacs while the RWB behavior is frequently detected in FSRQs (e.g., Gu et al. 2006; Zhang et al. 2018; Li et al. 2018; Gupta et al. 2019). Villata et al. (2002, 2004a) argued that the BWB relation

**Table 4** The Result of Color-magnitude Diagrams

Julian Date (JD)	Date (yyyy mm dd)	Color index	Magnitude	No.	Sc	$p$ -value	Correlation
2457696	2016 11 03	$R - V$	$V$	160	0.50	$6.6 \times 10^{-12}$	strong
2457697	2016 11 04	$R - V$	$V$	93	0.43	$1.3 \times 10^{-5}$	strong
2457745	2016 12 22	$R - V$	$V$	95	0.48	$6.3 \times 10^{-7}$	strong
		$R - B$	$B$	95	0.64	$1.3 \times 10^{-12}$	strong
		$V - B$	$B$	97	0.64	$1.5 \times 10^{-12}$	strong
2457746	2016 12 23	$R - V$	$V$	101	0.54	$6.5 \times 10^{-9}$	strong
		$R - B$	$B$	101	0.66	$4.6 \times 10^{-14}$	strong
		$V - B$	$B$	101	0.54	$3.0 \times 10^{-9}$	strong
2458012	2017 09 15	$I - R$	$R$	233	0.26	$6.9 \times 10^{-5}$	strong
		$R - B$	$B$	232	0.62	$4.5 \times 10^{-26}$	strong
		$I - B$	$B$	232	0.71	$1.0 \times 10^{-36}$	strong
2458013	2017 09 16	$I - R$	$R$	232	0.36	$1.2 \times 10^{-8}$	strong
		$R - B$	$B$	235	0.46	$7.1 \times 10^{-14}$	strong
		$I - B$	$B$	235	0.57	$4.1 \times 10^{-21}$	strong
2458014	2017 09 17	$I - R$	$I$	228	0.12	$7.9 \times 10^{-2}$	no
		$R - B$	$B$	230	0.04	$5.6 \times 10^{-1}$	no
		$I - B$	$B$	228	0.04	$5.7 \times 10^{-1}$	no
2458369	2018 09 07	$B - I$	$B$	31	0.65	$1.0 \times 10^{-4}$	strong
2458370	2018 09 08	$B - R$	$B$	52	0.62	$9.5 \times 10^{-7}$	strong
		$B - I$	$B$	52	0.42	$2.1 \times 10^{-3}$	strong
2458420	2018 10 28	$R - V$	$V$	68	0.70	$2.8 \times 10^{-11}$	strong
		$R - B$	$B$	67	0.82	$9.5 \times 10^{-18}$	strong
		$V - B$	$B$	67	0.64	$4.6 \times 10^{-9}$	strong
2458424	2018 11 01	$I - R$	$R$	132	0.36	$1.8 \times 10^{-6}$	strong
2458425	2018 11 02	$R - V$	$V$	84	0.26	$1.9 \times 10^{-2}$	mild
		$R - B$	$B$	84	0.58	$7.7 \times 10^{-9}$	strong
		$V - B$	$B$	84	0.49	$1.8 \times 10^{-6}$	strong
2458456	2018 12 03	$R - V$	$V$	51	0.49	$1.8 \times 10^{-1}$	no
		$R - B$	$B$	51	0.20	$2.6 \times 10^{-1}$	no
		$V - B$	$B$	51	0.21	$3.0 \times 10^{-4}$	weak

was more likely to be detected in short isolated outbursts. The BWB trend of BL Lacertae has been detected in a number of previous research efforts (Racine 1970; Speziali & Natali 1998; Vagnetti & Trevese 2003; Stalin et al. 2006; Papadakis et al. 2007; Ikejiri et al. 2011; Gaur et al. 2015; Wierzcholska et al. 2015; Meng et al. 2018). Our intra-day color-magnitude results are consistent with most of the historical observations.

#### 4 DISCUSSIONS AND CONCLUSIONS

We monitored BL Lacertae in the  $B$ ,  $V$ ,  $R$  and  $I$  bands for 14 nights during 2016-2018. The object manifested IDV in 23 light curves on 12 nights.

It has been found that the IDV amplitude of BL Lacertae is greater at higher frequencies (e.g., Kurtanidze et al. 2001; Fan et al. 2001; Papadakis et al. 2003; Hu et al. 2006; Gaur et al. 2015; Meng et al. 2017). This behavior has also been detected in our observation. Butuzova (2021) found similar behavior for S5 0716+714. Gaur et al. (2015) interpreted this behavior as higher energy electrons accelerated by the shock front lose energy faster than low energy electrons through synchrotron radiation. Hence higher frequency photons produced by these electrons will have a more violent change than lower frequency photons.

This will be observed as IDV amplitude being greater at higher frequencies. The higher energy electrons are produced in a thin layer behind the shock front and lower-frequency emission is spread out behind the shock front (Marscher & Gear 1985), which results in time lags in the peak of the light curve toward lower frequencies. However, this trend is not universal in every observation. The flux of bluer bands is lower than that in redder bands and also has higher errors than in redder bands (Fig. 3 affirms that the magnitude of  $B$  band is larger than that in  $R$  band for BL Lacertae). The error component in Equation (3) will reduce the IDV amplitude, so the IDV amplitude of bluer bands with higher errors will be reduced more than the IDV amplitude of redder bands. For example on 2017 September 16 (JD 2458013),  $R$  and  $I$  have comparable IDV amplitudes.

A BWB trend was found in our observation. This is consistent with previous studies (e.g., Vagnetti & Trevese 2003; Gaur et al. 2015; Wierzcholska et al. 2015; Meng et al. 2017; Zhang et al. 2018; Gaur et al. 2017; Bhatta & Webb 2018; Zhai & Wei 2012). We did not subtract the contribution of the host galaxy from the total flux since Villata et al. (2002) concluded that the color changes are an intrinsic property of fast flares and are not related to the host galaxy contribution. Hu et al. (2006) also

argued that the host galaxy and AGN have similar color so the color changes of an AGN are not affected by its host galaxy. Wierzcholska et al. (2015) did a long-term observation of BL Lacs and argued that the BWB trend is less likely caused by the host galaxy if the color-magnitude diagram shows separate branches. It is believed that the BWB trend originated from the emission regions of the jet. As the object gets brighter, more relativistic electrons will be accelerated and injected into the emission zone. The high energy photons from the synchrotron mechanism typically emerge sooner and closer to the shock front than the lower energy ones, thus causing color variations and larger variation amplitude at higher frequencies (Chiang & Böttcher 2002; Fiorucci et al. 2004). According to Feng et al. (2020), the significance of the BWB trend might be affected by the strength of variation, and the BWB trend caused by the shock will be more significant during a weaker phase of variation and vice versa.

No time lag has been detected in our observation. Wu et al. (2012) mentioned four key parameters that might determine whether the time lag can be detected: wavelength separation, variation amplitude, temporal resolution and measurement accuracy. According to Table 1, our temporal resolution (less than 5 minutes) is much smaller than the previously detected time lag. Three or four filters were employed to observe BL Lacertae on 10 nights which provided us large wavelength separation. Small variation amplitude (JD 2457697) and low measurement accuracy (JD 2458420, JD 2458424) might be the reason why we did not detect time lag. In addition, correlation analysis will fail to detect the time lag (if there is any) between featureless or monotonically brightening or darkening light curves, such as those of JD 2457696, 2458012 and 2458014.

In conclusion, BL Lacertae showed IDV in 23 light curves on 12 nights among our 14 nights of observation during 2016–2018. We found the IDV amplitude of BL Lacertae is greater at higher frequencies. In addition, BL Lacertae displayed a BWB trend on most of the nights. Finally, no time lag has been detected in our observation.

**Acknowledgements** This work has been supported by the National Natural Science Foundation of China (Grant No. 11973017).

## References

- Abdo, A. A., Ackermann, M., Agudo, I., et al. 2010, *ApJ*, 716, 30
- Agarwal, A., & Gupta, A. C. 2015, *MNRAS*, 450, 541
- Alexander, T. 1997, Is AGN Variability Correlated with Other AGN Properties? ZDCF Analysis of Small Samples of Sparse Light Curves, in *Astronomical Time Series*, eds. D. Maoz, A. Sternberg, & E. M. Leibowitz, 218, 163
- Alexander, T. 2013, arXiv e-prints (arXiv:1302.1508)
- Bach, U., Villata, M., Raiteri, C. M., et al. 2006, *A&A*, 456, 105
- Bhatta, G., & Webb, J. 2018, *Galaxies*, 6, 2
- Böttcher, M., Marscher, A. P., Rivasio, M., et al. 2003, *ApJ*, 596, 847
- Butuzova, M. S. 2021, *Astroparticle Physics*, 129, 102577
- Carini, M. T., Miller, H. R., Noble, J. C., & Goodrich, B. D. 1992, *AJ*, 104, 15
- Chiang, J., & Böttcher, M. 2002, *ApJ*, 564, 92
- Ciprini, S., Tosti, G., Teräsanta, H., & Aller, H. D. 2004, *MNRAS*, 348, 1379
- de Diego, J. A., Polednikova, J., Bongiovanni, A., et al. 2015, *AJ*, 150, 44
- Edelson, R. A., & Krolik, J. H. 1988, *ApJ*, 333, 646
- Epstein, E. E., Fogarty, W. G., Hackney, K. R., et al. 1972, *ApJL*, 178, L51
- Fan, J. H., & Lin, R. G. 1999, *ApJS*, 121, 131
- Fan, J. H., Qian, B. C., & Tao, J. 2001, *A&A*, 369, 758
- Feng, H.-C., Liu, H. T., Bai, J. M., et al. 2020, *ApJ*, 888, 30
- Fiorucci, M., Ciprini, S., & Tosti, G. 2004, *A&A*, 419, 25
- Fossati, G., Maraschi, L., Celotti, A., Comastri, A., & Ghisellini, G. 1998, *MNRAS*, 299, 433
- Gaskell, C. M., & Peterson, B. M. 1987, *ApJS*, 65, 1
- Gaur, H., Gupta, A., Bachev, R., et al. 2017, *Galaxies*, 5, 94
- Gaur, H., Gupta, A. C., Bachev, R., et al. 2015, *MNRAS*, 452, 4263
- Goyal, A., Mhaskey, M., Gopal-Krishna, et al. 2013, *Journal of Astrophysics and Astronomy*, 34, 273
- Gu, M. F., Lee, C. U., Pak, S., et al. 2006, *A&A*, 450, 39
- Gupta, A. C., & Joshi, U. C. 2005, *A&A*, 440, 855
- Gupta, A. C., Gaur, H., Wiita, P. J., et al. 2019, *AJ*, 157, 95
- Heidt, J., & Wagner, S. J. 1996, *A&A*, 305, 42
- Hu, S. M., Wu, J. H., Zhao, G., & Zhou, X. 2006, *MNRAS*, 373, 209
- Ikejiri, Y., Uemura, M., Sasada, M., et al. 2011, *PASJ*, 63, 639
- Kurtanidze, O. M., Richter, G. M., & Nikolashvili, M. G. 2001, in *Galaxies and their Constituents at the Highest Angular Resolutions*, ed. R. T. Schilizzi, 205, 82
- Li, X.-P., Luo, Y.-H., Yang, H.-T., et al. 2018, *RAA (Research in Astronomy and Astrophysics)*, 18, 150
- Marscher, A. P. 2014, *ApJ*, 780, 87
- Marscher, A. P., & Gear, W. K. 1985, *ApJ*, 298, 114
- Meng, N., Wu, J., Webb, J. R., Zhang, X., & Dai, Y. 2017, *MNRAS*, 469, 3588
- Meng, N., Zhang, X., Wu, J., Ma, J., & Zhou, X. 2018, *ApJS*, 237, 30
- Miller, J. S., & Hawley, S. A. 1977, *ApJL*, 212, L47
- Nesci, R., Maesano, M., Massaro, E., et al. 1998, *A&A*, 332, L1
- Nikolashvili, M. G., & Kurtanidze, O. M. 2004, *Nuclear Physics B Proceedings Supplements*, 132, 205
- Padovani, P., & Giommi, P. 1995, *MNRAS*, 277, 1477
- Papadakis, I. E., Boumis, P., Samaritakis, V., & Papamastorakis,

- J. 2003, *A&A*, 397, 565
- Papadakis, I. E., Villata, M., & Raiteri, C. M. 2007, *A&A*, 470, 857
- Peterson, B. M., Wanders, I., Horne, K., et al. 1998, *PASP*, 110, 660
- Peterson, B. M., Ferrarese, L., Gilbert, K. M., et al. 2004, *ApJ*, 613, 682
- Racine, R. 1970, *ApJL*, 159, L99
- Raiteri, C. M., Villata, M., Capetti, A., et al. 2009, *A&A*, 507, 769
- Sadun, A. C., Asadi-Zeydabadi, M., Hindman, L., & Moody, J. W. 2020, *Galaxies*, 8, 11
- Sandrinelli, A., Covino, S., Treves, A., et al. 2018, *A&A*, 615, A118
- Scarpa, R., Urry, C. M., Padovani, P., Calzetti, D., & O’Dowd, M. 2000, *ApJ*, 544, 258
- Smith, P. S., Balonek, T. J., Heckert, P. A., et al. 1985, *AJ*, 90, 1184
- Speziali, R., & Natali, G. 1998, *A&A*, 339, 382
- Stalin, C. S., Gopal-Krishna, Sagar, R., et al. 2006, *MNRAS*, 366, 1337
- Vagnetti, F., & Trevese, D. 2003, *Mem. Soc. Astron. Italiana*, 74, 963
- Villata, M., Raiteri, C. M., Kurtanidze, O. M., et al. 2002, *A&A*, 390, 407
- Villata, M., Raiteri, C. M., Kurtanidze, O. M., et al. 2004a, *A&A*, 421, 103
- Villata, M., Raiteri, C. M., Aller, H. D., et al. 2004b, *A&A*, 424, 497
- Wagner, S. J., & Witzel, A. 1995, *ARA&A*, 33, 163
- Webb, J. R., Freedman, I., Howard, E., et al. 1998, *AJ*, 115, 2244
- Wiercholska, A., Ostrowski, M., Stawarz, Ł., et al. 2015, *A&A*, 573, A69
- Wu, J., Böttcher, M., Zhou, X., et al. 2012, *AJ*, 143, 108
- Zhai, M., & Wei, J. Y. 2012, *A&A*, 538, A125
- Zhang, X., Wu, J., & Meng, N. 2018, *MNRAS*, 478, 3513